Received: 2 October 2019 | Revised: 1 March 2020 | Accepted: 1 April 2020

DOI: 10.1002/fam.2841

INTERFLAM SPECIAL ISSUE

WILEY

Spatiotemporal measurement of light extinction coefficients in compartment fires

Lukas Arnold[1,2] | Alexander Belt[1] | Thorsten Schultze[3] | Lea Sichma[3]

[1]Institute for Advanced Simulation, Forschungszentrum Jülich, Jülich, Germany

[2]Computational Civil Engineering, Bergische Universität Wuppertal, Wuppertal, Germany

[3]Communication Systems, University Duisburg-Essen, Duisburg, Germany

Correspondence
Lukas Arnold, Institute for Advanced Simulation, Forschungszentrum Jülich, Jülich, Germany.
Email: l.arnold@fz-juelich.de

Summary

In case of fire, the visibility plays a major role as it limits the occupants' orientation capabilities and the perception of signs. These effects are determined by the light extinction due to smoke or other aerosols produced in fires. The presented method is based on the optical observation of an array of light sources during a fire in a laboratory experiment. The smoke induced into the compartment leads to a drop in intensity of each individual light source. This information is used to deduce the extinction along the line-of-sight to the camera. Once the data are captured, an automated processing is used to locate the diodes on the images and determine their intensity. Here, the optical image of the small diodes is assumed to have a known shape, so that the optimisation algorithm is capable to identify the location of the diode's centre and quantify the luminosity in a sub-pixel range. The result is a time series for each diode, indicating the change of the relative luminosity, w.r.t. the initial values. Finally, a model for the extinction along each line-of-sight is formulated. It assumes that the light extinction coefficient is distributed in homogeneous layers. The number of layers is a free model parameter. Given this spatial distribution of the extinction coefficient and the experimental geometry, each line-of-sight is impacted by a number of layers, of yet unknown coefficient values. An inverse modelling approach is used here to find coefficient values that match the modelled line-of-sight extinction with the observed luminosity drops. The final result is a time- and height-dependent distribution of the light extinction coefficient during the full experiment.

1 | INTRODUCTION

In the assessment of life safety in complex building structures in case of fire visibility is one of the main tenability criteria in performance-based design. Especially if the orientation of the occupants depends on the perception of signs and doors,[1] a sufficient visibility is crucial. Both aspects, that is, visibility as a tenability criterion and as a limiting factor for the orientation, manifest in the ASET-RSET[2] concept. Here, visibility will reduce the available safe egress time[3,4] and due to reduction of walking speed or prolonged orientation and route evaluation,[5] it will increase the required safe egress time. As modern fire safety analysis is based on computer simulations, for example, using the fire dynamics simulator (FDS[6]), a valid prediction of the smoke spread and especially its light attenuation must be achieved. Past computations with FDS with the aim to validate the prediction of smoke density and light extinction, like References [7,8], indicate significant deviations and the need for further research.

The copyrightline for this article was changed on 19 December 2020 after original online publication.

The determination of visibility is basically based on a threshold for the intensity of the perceived light.[9] As the light travels from the object, for example, an illuminated sign, to the observer, its intensity may be reduced due to an interaction with the medium between both. The kind of interaction, for example, scattering or absorption, as well as its amplitude and dependence on wavelength are subject to the type and number of particles in the medium. While the particle density n has mainly an impact on the amplitude, the predominant is given by the properties of the particles. The latter aspect is effectively described by an interaction, here mainly the extinction cross-section c_{ext}. Its value and the value of quantities defined further down depend on the wavelength of the light. However, this will not be further distinguished in this article and implicitly assumed that they all are wavelength dependent, without additional indexing or labelling in the text.

As a light ray travels along the line-of-sight, its initial intensity I_0 is in general reduced. The transmission T describes the ratio of the reduced intensity I and I_0. Using the Beer-Lambert law (equation 1, cf.[10]), the transmission of monochromatic light can be expressed as a function of the optical depth τ.

$$T = \frac{I}{I_0} = \exp(-\tau). \tag{1}$$

In a homogeneous medium with a particle density n and an extinction cross-section c_{ext} the optical depth τ is proportional to the distance along the line-of-sight Δs (Equation 2).

$$\tau = c_{ext} \cdot n \cdot \Delta s = \sigma \cdot \Delta s. \tag{2}$$

A further simplification is the definition of the extinction coefficient σ, which represents the product of n and c_{ext} (see Equation (2)). This leads to only a single physical quantity to be measured in order to describe the light attenuation, as the other one, the distance Δs, is purely geometrical. A summary of the relevant processes and optical properties of smoke can be found in the SFPE handbook of fire protection engineering.[11,12] It should be noted that the reported extinction coefficients in the SFPE handbook are close to constant and depend only on the type of combustion, that is, flaming vs smouldering.

A common approach to measure the light extinction is an apparatus that combines a light transmitter and receiver. Eventually, both are close to each other, while a light beam is sent out and reflected back with a mirror. This is the basic setup of the MIREX[13] measurement system. It uses infrared light, which is send across a distance of 2 m. The specification for the light spectrum is that 50% of the power is emitted between 800 and 950 nm. This apparatus can be used to precisely measure the light extinction at a localised, yet 1 m wide, position. The usage of multiple devices would allow a spatially resolved measurement; however, it would increase the cost and impact the fluid dynamics due to the physical extension of the apparatus. However, the measured data can be used for localised comparison with the results of the presented approach. Fundamental challenges and uncertainties in the cause of experimentally investigating the light extinction and scattering during compartment fires are outlined in References [14,15].

In this article, a simple technique to measure the extinction coefficients σ in the range of visible light is proposed. The implicit measurement leads to spatially, here in vertical direction, and temporally resolved data. One of the fundamental assumptions is a layered structure of the smoke. The final goal is to provide spatiotemporal data as a validation basis for the computation of light extinction processes in compartment fires. A validation case, similar to Reference [16], will be conducted in future work.

The outline of this article is as follows. First, one of the conducted experiments is presented. Its data will be used as example data for the following methodology section. The presented methodology is split into the raw data capturing, the data post-processing and the determination of the extinction coefficients. Finally, two application examples are shown and conclusions and future work are stated.

2 | EXPERIMENTAL SET-UP

This section outlines the main characteristics of the experimental setup. The experimental data are used in the following sections to demonstrate the methodology and to provide an application example. The experiment took place in the Heinz-Luck fire detection laboratory

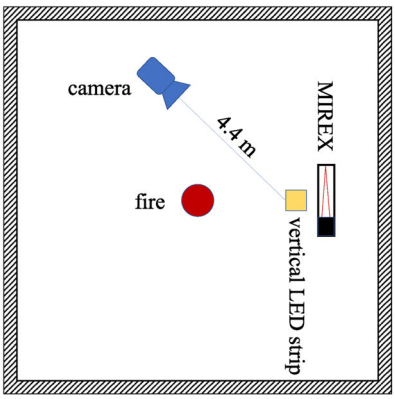

(A) Floor plan of the experimental setup. The main objects are the pool fire, the LED-strip, the MIREX and the camera.

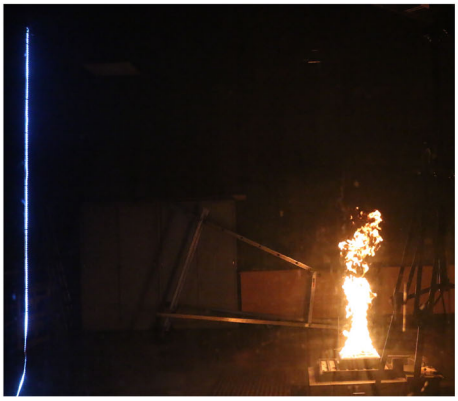

(B) Impression of test fire TF5. The LED strip is visible, while the camera is located on the right hand side.

FIGURE 1 Experimental setup following the European standard EN 54

at the university of Duisburg-Essen, Germany. The compartment is of cuboid shape with a variable ceiling height. The wall-to-wall distances are about 10 m, while the ceiling height was chosen to 3.37 m. As the hall is mainly used for testing purposes following the European standard EN 54,[17] the laboratory conditions are well known and the presented setup is similar to it. Figure 1A depicts the location of the objects of interest: a pool fire, a camera, a MIREX apparatus and a vertical LED strip. In the following, only the placement of the camera is important, which is at a height of 2.3 m and at a distance of 4.4 m from the LED strip. A photo of one of the experiments is shown in Figure 1B.

The LED strip used in the experiment is a common consumer product. It is build out of 5 cm long parts that contain three LED units (see Figure 2A). The units separation distance is 5/3 cm, that is, about 1.67 cm. Each of the units has three individual LEDs that emit red, green and blue light and are therefore capable to produce light in combination of those (see Figure 2B). In addition, it is possible to control the intensity of a LED. In the presented experiments, the LED units are set to white, that is, all LEDs are on, with the maximal intensity. The length of the vertically aligned strip was 2.35 m, starting about 5 cm below the ceiling, and it contained 141 LED units.

The fire was one of the fires defined in EN 54 as TF5. It is a pool fire with *n*-heptane as fuel. In contrast to the norm, the amount of fuel was reduced to 500 g, which lead to a burning duration of about 3 minutes. The choice of this fire type is due to the fact that it is the most simple one to be modelled with numerical simulation methods, as it does not involve pyrolysis and the combustion reaction is consuming a single pure fuel.

Figure 3 shows the time line of the experimental procedure. The timing in this run was as follows:

- t = 0 seconds start of the experiment
- t~30 seconds ignition of the pool fire
- t~200 seconds all fuel is consumed, the fire is off
- t~420 seconds hall's ventilation system is turned on
- t~1200 seconds end of the measurements, end of the experiment

The examples in the following methodology section are based on experimental data gathered in the above-stated experimental run.

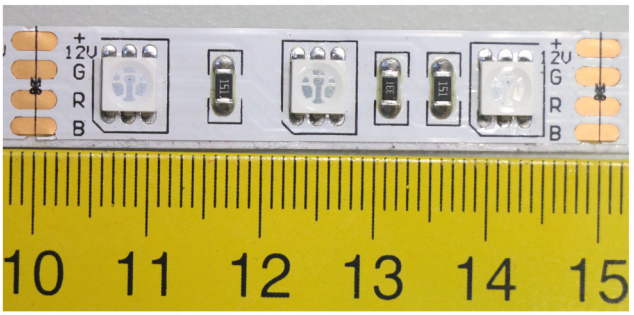

(A) LED turned off. Length units are in cm

(B) LED turned on

FIGURE 2 Physical extension of a LED unit and location of the LED dots

3 | METHODOLOGY

The presented methodology is split into three aspects. The first subsection outlines a few recommendations of the raw data acquisition, while the second one describes the procedure to model the image of each LED unit and thus find its position and determine its intensity in an image frame. In the last subsection, a method to discretise the compartment volume into homogeneous smoke layers and the determination of the light attenuation coefficients is introduced.

3.1 | Raw data acquisition

The methodology is based on the analysis of photo images captured by a camera. During the experiment, the camera continuously

- $t = 0\,\mathrm{s}$ start of the experiment
- $t \sim 30\,\mathrm{s}$ ignition of the pool fire
- $t \sim 200\,\mathrm{s}$ all fuel is consumed, the fire is off
- $t \sim 420\,\mathrm{s}$ hall's ventilation system is turned on
- $t \sim 1200\,\mathrm{s}$ end of the measurements, end of the experiment

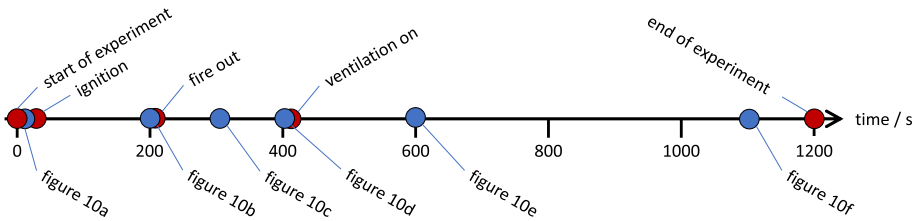

FIGURE 3 Time line of the experimental procedure. The red dots indicate important time points of the experiment, while the blue ones show the time points of Figure 10

captures the LED strip. As the scientific quality of the images is crucial, the settings of the camera are stated and discussed here.

The used camera was a Canon 80D with a Canon 18 to 35 mm lens. It was run in full manual mode, that is, without any brightness corrections or other adjustments. The choice of a manual mode is important as otherwise the camera would adjust its parameters in order to take well-balanced images. This would introduce luminosity changes of the LEDs, which are not due to light attenuation but due to changes in the camera settings. The images are stored in the common jpeg format as well as in a raw format. The latter one can be used to further increase the accuracy of the analysis as it offers a higher luminosity resolution.

In the manual mode of the camera, all relevant parameters must be manually set. The objective is to have all LED units in focus and the image of the initial signal should be as bright as possible without saturating the CCD chip. In this specific setup, the focal ratio was set to 16 in order to achieve a long depth of field, that is, have all LED units in focus. With a low ISO number of 100—to reduce the CCD noise—the resulting exposure time was 1/500 seconds. With a distance to the LED strip of about 4.4 m and a focal length of 18 mm, each pixel of the image corresponds to a distance of about 0.88 mm on the LED strip. Using a programmable remote control, the camera took a picture every second.

Figure 4 shows a part of a baseline image, that is, taken just before the experiment started. Each colour image is a combination of three channels, representing the red, green and blue colour contributions. The very left subfigure shows the common RGB (red/green/blue) representation of the image and the other figures depict the individual channels. The value range, here of the jpeg file format, uses 256 integer values for each channel. The red and green channels do not reach the saturation value of 255; however, the blue one is reaching this value and is therefore saturated. Here, the blue channel cannot be used for a scientific evaluation as the actual brightness level is not captured by the CCD.

3.2 | Determination of LED dot positions

Once the images are taken, the position and intensity of all LED units needs to be found. This is done in two phases: First, and only once per experiment, search areas are fixed. Second, an image model is fitted to each individual image of all LED units. The result is a list with various properties, like intensity or position, for all units on the strip. In the following, the analysis is demonstrated only for one, here red, channel.

In the first phase, search areas for each LED unit are identified. This is done only once and is based on a reference image, for example, taken just before the experiment started. It is assumed that all available LED units are clearly visible on the image. Here, a simple maximum search is conducted. For the found maximum a pixel range, the search area, is defined. This area is excluded during the search for the next maximum. This procedure is repeated until all maxima, which are well above the mean value, are found. The width of the search area depends on the pixel separation of the LED units on the image. In the presented case, the width was set to 20 pixel. To ease the automated analysis, it is possible to exclude defect or partly covered LED units from further analysis. It should be noted that the definition of the search areas must happen on the reference frame as during the experiment the LED unit image may become very dark or even vanish. In this case, the analysis would miss the important information of an highly attenuated signal.

In the second phase, a simple image model for a single LED unit is fitted to the individual search areas. The model is based on the assumption that the image can be represented by an algebraic function. The basic structure of the function is as follows. There is a region around the central point at x_0 and y_0 with a nearly constant brightness amplitude A_0. The central region has a radius r_0 and transits smoothly towards zero within the width w. However, the LED unit images are asymmetric. Therefore, the radius r_0 and the width w can be defined as two components in the x- and y-direction, that is, $r_{0,x}$, $r_{0,y}$, w_x and w_y. In addition, a rotational angle α can be defined. In total there are eight parameters: A_0, x_0, y_0, $r_{0,x}$, $r_{0,y}$, w_x, w_y and α. The explicit formula for the value A_m of a pixel at position x, y in the model image is given in Equation (3).

$$A_m(x,y) = A_0 \cdot \frac{1}{2}\left(1-\tanh\left(\frac{r(x,y)-r_0(x,y)}{w(x,y)}\right)\right). \tag{3}$$

With the radius r defined as

$$r(x,y) = \sqrt{(x-x_0)^2+(y-y_0)^2} \tag{4}$$

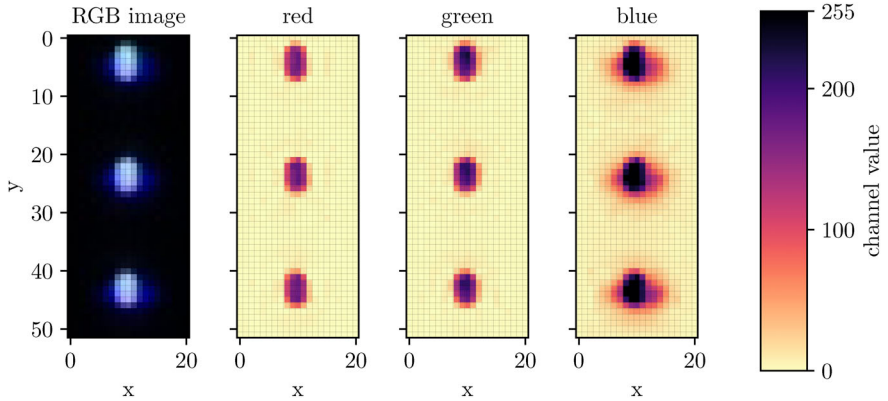

FIGURE 4 Zoomed area of three LED units on a reference image frame. The image on the very left shows the combined RGB colour image, while the following ones show the individual colour channels

and the polar angle ϕ

$$\phi(x,y) = \arctan\left(\frac{y}{x}\right) + \alpha \quad \text{with the according quadrant adoptions} \tag{5}$$

the central region $r_0(x, y)$ and the width $w(x, y)$ can be computed as a function of the above-defined polar coordinates

$$r_0(x,y) = \frac{r_{0,x} r_{0,y}}{\sqrt{(\sin(\phi) r_{0,x})^2 + (\cos(\phi) r_{0,y})^2}}, \tag{6}$$

$$w(x,y) = \frac{w_x w_y}{\sqrt{(\sin(\phi) w_x)^2 + (\cos(\phi) w_y)^2}}. \tag{7}$$

Figure 5 provides three examples of Equation (3). It demonstrates a symmetric image with an extended central region (left), an inclined asymmetric image (middle) and a blurred image (right).

To find the best fitting parameters, a minimisation algorithm is used. The cost function Ω_{LED} is the L2-norm of the pixel values (one channel) of the experimental image A_e within the search area and the modelled intensity $A_m(x, y)$ on the same pixel area:

$$\Omega_{\text{LED}} = \sqrt{\sum_{\text{all pixels } i,j} (A_e(i,j) - A_m(i,j))^2}. \tag{8}$$

In addition, penalty terms are defined to ensure that the central points are within the search area and the amplitude, radii and widths are positive.

Figure 6 shows an example, where an individual LED unit image (left) is fitted by the model image (middle). The best fitting parameter values for this LED unit image are $x_0 = 11.01$, $y_0 = 12.32$, $r_{0,x} = 1.75$, $r_{0,y} = 2.91$, $A_0 = 170.11$, $w_x = 0.77$, $w_y = 0.72$, $\alpha = 0$. The overlay of both images (right) illustrates the reasonable matching of the original image. It should be noted that this approach is capable of detecting small movements and changes in the intensity, as the model is not bound to the discrete channel and position, that is, pixel, values.

Finally, this process is repeated for all LED units and all frames taken. The results are time lines for each model parameter of each LED unit. To demonstrate the resulting data, a few selected time lines for three LED units, located at a low, middle and upper position on the LED strip, are shown in Figure 7. Figure 7A shows the change in the amplitude A_0 during the experiment. The LED unit at the upper position shows the largest drop in intensity. The y-coordinate of the central point y_0, Figure 7B, shifts synchronously for all LED units on a scale of two pixels in the captured frames, yet a clear dynamics is detectable. While the parameters $r_{0,y}$ and w_y of LED unit in the lower position show only little change, the other ones show an evolution along the course of the experiment. In both cases, the central region becomes smaller while the transition region grows, that is, the shape becomes refocused. Towards the end of the time series, the values of all parameters and LED units tend towards the initial values.

3.3 | Computation of extinction coefficients

The final goal of the presented method is to gain spatially resolved information of the extinction coefficients. As described in the following, a simple model based on spatial discretisation, here in horizontal layers, is outlined. Using the captured intensities, based on the amplitude parameter A_0 in Equation (3), a best matching set of extinction coefficients is determined. This approach applies the line-of-sight integral of the Beer-Lambert law in an inhomogeneous medium.

The proposed model has the following assumptions:

1. the light absorption properties, that is, σ, in a layer is homogeneous,
2. the plume region is neglected,
3. light paths are linear, for example, refraction due to varying gas temperatures is neglected, and
4. only the product $\sigma = c_{\text{ext}} \cdot n$ in Equation (2) is determined.

The severity of these assumptions is different for each one. While the assumption of homogeneous layers may be critical for complex compartments, neglecting of the plume region will be a minor issue for sufficiently large spaces. Refraction will have a minor role for low energy fires, like smouldering, as the involved temperatures are just above the ambient. Finally, the capability to distinguish between c_{ext} and n is not critical for the computation of visibility, as the optical depth depends only of their product σ.

The model's data structure is a set of N_{layers} extinction coefficients σ_i. They represent the values at homogeneous horizontal layers, which fill the domain of interest, for example, a compartment (see Figure 8). As the light rays travel from one of the N_{LEDs} LED units L_j to the camera, it passes one or more of the layers. The height of the

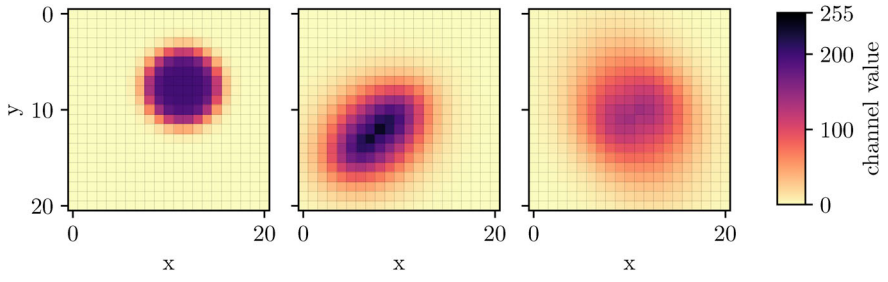

FIGURE 5 Examples of Equation (3)

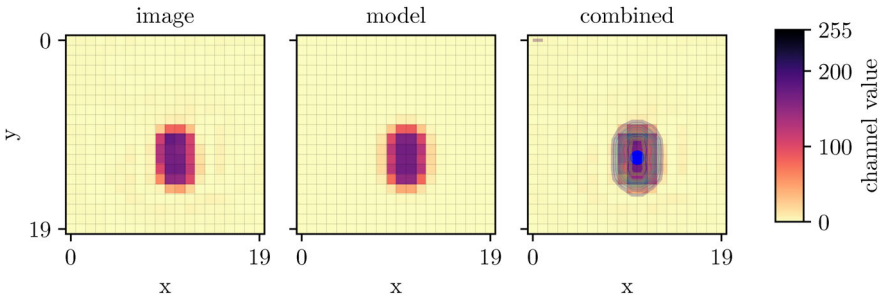

FIGURE 6 Fitting example for a single LED unit

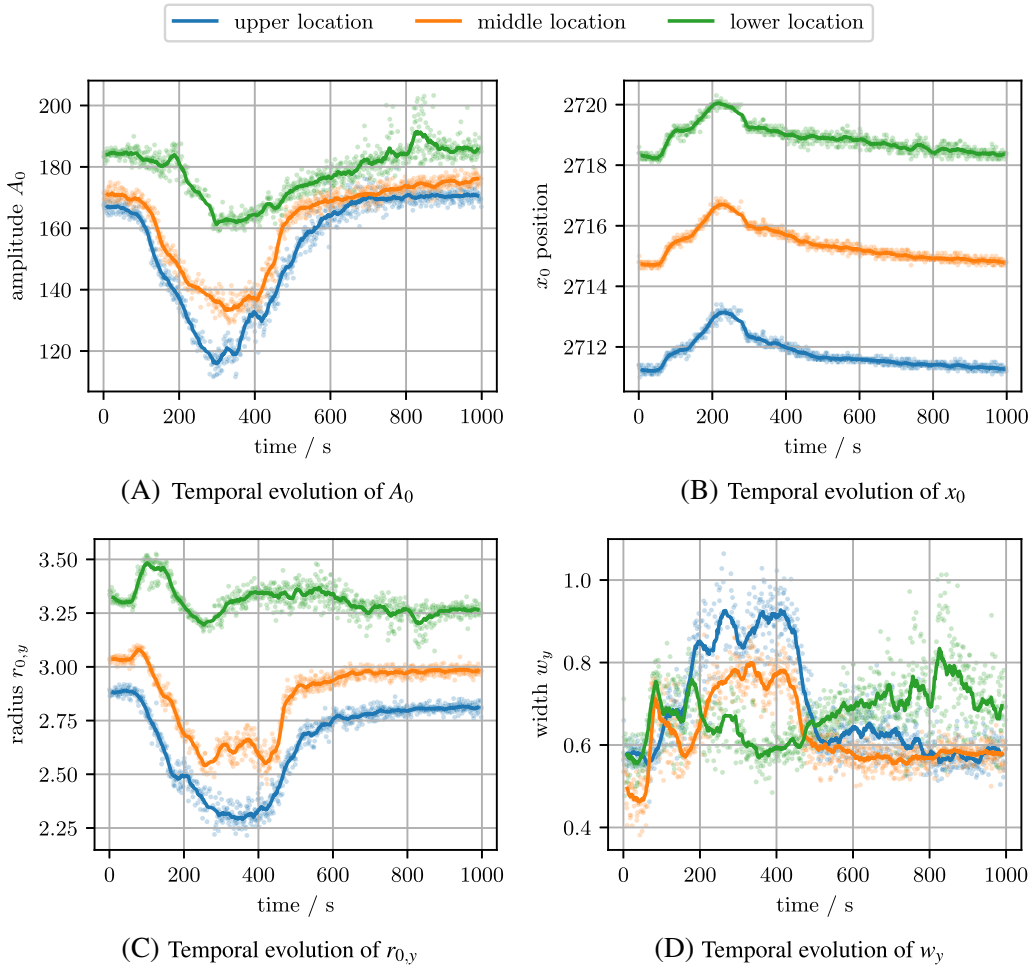

FIGURE 7 Temporal evolution of model parameters for three selected LED units

layers Δh_i does not have to be equal; however, it is kept constant in this contribution. The value of N_{layers} represents a kind of spatial resolution with respect to height. However, increasing this number will not lead to better results, as it reduces the amount of available information per layer during the optimisation process outlined later on.

In order to evaluate the Beer-Lambert law, the path of each straight light ray across the layers has to be determined. The path between the camera and the LED unit L_j is computed using fundamental geometry. This results in path lengths $\Delta s_{i,j}$ for the light ray travelling from the jth LED unit thought the ith layer. If the light ray does not cross a layer, the corresponding value is set to zero.

The determination of the extinction coefficients σ_i is based on the general form of the Beer-Lambert law for an inhomogeneous medium. Equation (9) demonstrates the integration along the path s.

$$\tau = \int_s c_{\text{ext}} n(s)\, ds = \int_s \sigma(s)\, ds. \tag{9}$$

The usage of discrete layers with constant values simplifies this integral into a finite sum over all layers, using the computed travel paths $\Delta s_{i,j}$ and the yet to be determined extinction coefficients σ_i (see Equation (10)).

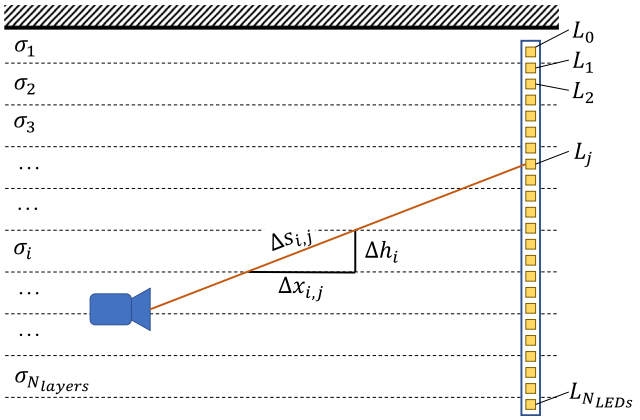

FIGURE 8 Schematics of the layer model. Each layer corresponds to a constant extinction coefficient σ_i. The LED units L_j are not aligned to these layers. The light rays from a LED unit to the camera pass individual layers, where $\Delta s_{i,j}$ indicates the path length travelled by the light emitted by the unit L_j in the ith layer

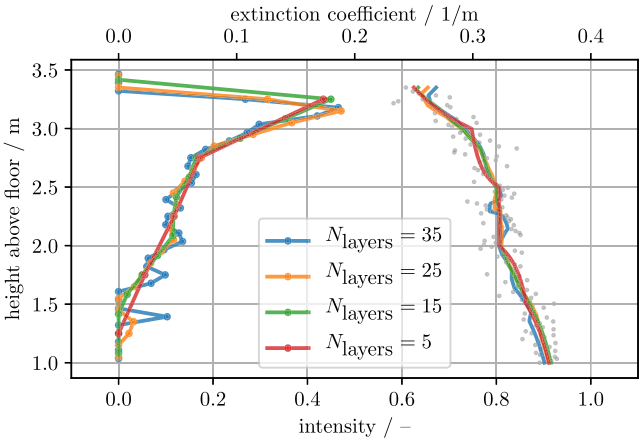

FIGURE 9 Comparison of models with varying number of layers N_{layers}. The lines on the left correspond to the extinction coefficients, while those on the right show the model output for the LED unit intensity I_m. Experimental intensities I_e are represented by grey dots

$$\tau_j = \sum_{i=1}^{N_{\text{layers}}} \sigma_i \Delta s_{i,j}. \tag{10}$$

In the following all intensities are scaled to their initial values I_0 and thus range from zero to one. The experimental intensities I_e are scaled by the mean of 10 reference images taken just before the experiment started. The modelled intensities $I_{m,\,j}$ of L_j are given by Equation (11).

$$I_{m,j} = \exp\left(- \sum_{i=1}^{N_{\text{layers}}} \sigma_i \Delta s_{i,j} \right). \tag{11}$$

Equation (12) poses an equation system, containing N_{LEDs} nonlinear equations, to be solved for σ_i. This system has to be solved for each frame; however, the travel paths $\Delta s_{i,\,j}$ are computed only once, as they do not change in time.

$$I_{m,j}\left(\sigma_0, \ldots, \sigma_{N_{\text{layers}}}\right) = I_{e,j} \quad \text{for all} j \in [1, N_{\text{LEDs}}]. \tag{12}$$

In order to solve the target equation system, a minimisation procedure is used. This has the advantage that additional criteria, but solely the distance between the experimental and modelled data, can be defined. Therefore, a cost function Ω_σ is defined as shown in Equation (13).

$$\Omega_\sigma = \sum_{j=1}^{N_{\text{LEDs}}} \left(I_{m,j} - I_{e,j}\right)^2 + \phi_s \sum_{i=2}^{N_{\text{layers}}-1} \left(\sigma_{i-1} - 2\sigma_i + \sigma_{i+1}\right) + \phi_a \sum_{i=1}^{N_{\text{layers}}} \sigma_i. \tag{13}$$

It is a sum of three contributions. The first one computes the L2-norm between the experimental and modelled data for all LED units. The second one represents the requirement of a smoothness of the solution, here the numerical approximation of the second derivative. In order to prevent individual high peaks, the weighting factor ϕ_s can be set to a non-trivial positive value to favour low curvatures. The last term controls if the minimisation process prefers high or low values of the extinction coefficients, depending of the sign of the weighting factor ϕ_a. This option is essential to capture a range of possible values for σ_i in cases where there is little impact on the L2-norm. For example, if the LED signal was damped to nearly zero, there is a minimal value for the extinction coefficient to achieve these results. However, the actual value may be significantly higher. In order to quantify these effects, the sign of ϕ_a can be accordingly chosen.

An example of the outcome of the above optimisation procedure is given in Figure 9. This figure contains a set of results, which are distinguished by the number of extinction coefficient layers N_{layers} in Equation (10). For each of the results, the vertical distribution of extinction coefficients is shown (left-hand side) as well as the corresponding modelled intensity I_m (right-hand side). First, the model is capable to represent the experimental intensities (grey dots) within the variation of the data. All N_{layers} lead to very similar curves. Second, also the extinction coefficients follow a similar shape. The curves with higher numbers of layers show more features, which are not necessary physical but may be artefacts of a more accurate fitting of the noisy data. Third, the extinction coefficients above about 3.35 m drop towards zero. This is due to the fact that the cost function, Equation (13), favours small extinction coefficients. As there is no experimental data for this heights—the top LED unit is at about 3.35 m—this leads to small or even zero coefficients. Each layer of the low N_{layers} numbers covers a larger portion of the space and therefore does not include layers, which are not crossed by any light paths.

4 | APPLICATION EXAMPLE

As the focus of this contribution is the methodology, this section presents just two selected aspects of the data analysis. These are the temporal evolution of the extinction coefficient layers and the comparison to a MIREX measurement.

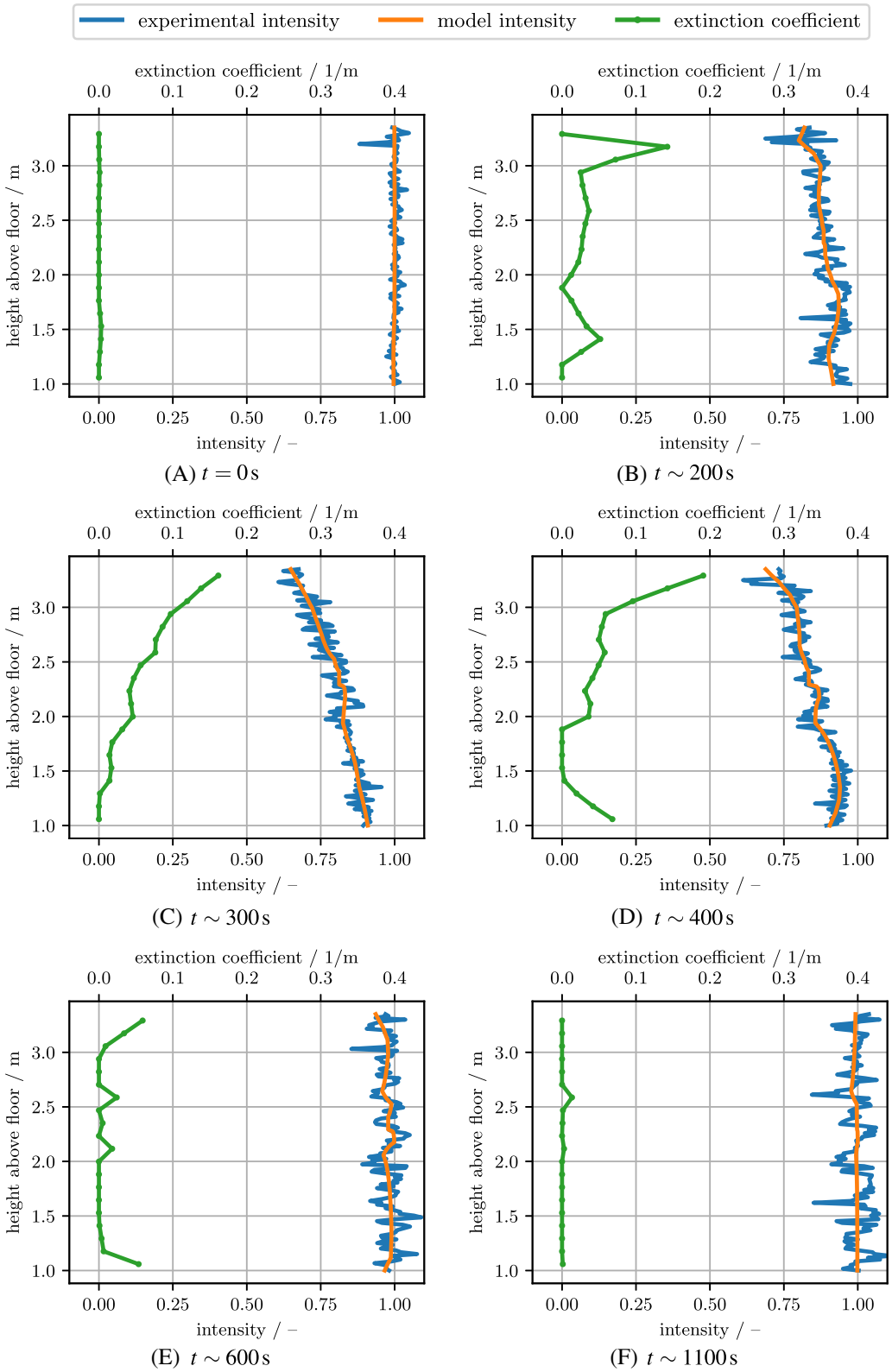

FIGURE 10 Temporal evolution of the extinction coefficient layers at six selected points in time (see Figure 3). The experimental intensity indicates the normalised LED values, while the model intensity is the result of a light path integration along the model layers with the according extinction coefficients

First, the development of the light attenuation in the layers is depicted in Figure 10 for six selected points in time. The selected times are outlined in Figure 3 and are chosen to capture the main dynamic of the experiment. At the beginning of the experiment, that is, t = 0 seconds, all extinction coefficients are nearly zero. The following three snapshots show a build-up of a layer with increasing

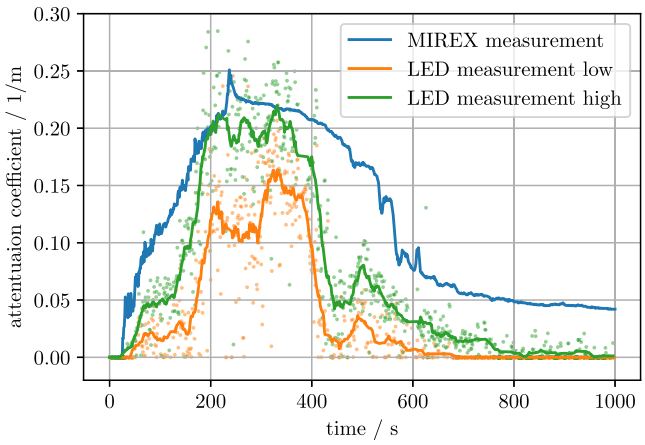

FIGURE 11 Comparison of a MIREX measurement with the results of the presented approach. The data based on the LED measurement shows the results of an optimisation towards low as well as high extinction coefficients

extinction coefficients. Especially at t~300 seconds, a layering with a smooth shape from zero at the lower layers towards the maximum at the highest point can be observed. Once the ventilation system is activated, the layering is significantly reduced (t~600 seconds) and eventually drops to the initial (zero) state, as shown for t~1100 seconds. Although this experiment does not provide new insights, this result demonstrates the capturing of the spatiotemporal evolution of the extinction coefficient.

Second, the results of the data analysis are compared with MIREX measurements. It is important to note that the data are not directly comparable as the MIREX measures the light extinction in the infrared regime, while the results shown here are for red light. However, nevertheless, both measurements are compared to identify trends and orders of magnitude. Figure 11 shows the temporal evolution of the extinction coefficient measured by the MIREX and of the new approach at the position—here the height—of the MIREX. In this figure, two datasets of the measurements based on the LED technique are shown. One is the result of an optimisation, where low extinction coefficients are favoured, positive ϕ_a in Equation (13). A second one where high values are favoured, negative ϕ_a. This is necessary as the MIREX is located just above the ceiling, that is, in the top layers of the model which have the highest uncertainty as only a few light paths cross them. With this approach, a kind of upper and lower limit for the extinction coefficients is estimated, where both limits still lead to reasonable representation of the experimental data. The comparison of both measurements demonstrates that the proposed method is able to capture the dynamics as well as the amplitude of the extinction coefficient the same way as the MIREX measurement. However, the MIREX system seems to be more sensitive, that is, indicates higher extinction coefficients, in the initial phase and in the decaying phase.

5 | CONCLUSIONS

This article presents an approach to capture the light attenuation of individual LED units in a compartment fire. Using this approach, multiple quantities, like mainly the amplitude but also the position and widening of the signal, can be captured on a scale, which are finer than the colour level or the pixel width. This accuracy allows to include further effects, like refraction, into the analysis. The determination of the extinction coefficients is based on a simple method and is therefore expected to be robust with respect to the failure of individual LEDs or small movements of the strip. However, the validation needs further investigation to find a more conclusive comparison method with other techniques. Although the comparison with the MIREX data is promising, more suitable measurement locations must be revised as well as the impact of the wavelength, here between infrared and red, must be evaluated. Eventually, the analysis with the LED light, which targets wavelengths in the visible spectrum, may lead to more applicable extinction coefficients.

The instantaneous capturing of spatially resolved extinction coefficients, especially in the visible spectrum, will provide a validation basis for numerical tools. Especially as it generates data for inhomogeneous distributions, so that transport processes can be evaluated as well. The general approach will allow an application on small scale as well as on large scale, as long as the assumptions are expected to be valid. This shows the need of providing a method to check the validity with experimental methods.

In terms of applicability, the proposed method is easily applicable at low cost. This is due to the usage of consumer products and no need for fine tuning or calibration with external sources. The most part of the process is covered by the data analysis. As the analysis is written in Python and can be freely shared with others—please contact the authors to gain access—it can be directly applied by others researchers.

6 | OUTLOOK

As pointed out in the conclusions, there exists a range of topics to improve the validity and applicability of the proposed method and a few of them are subject of current research.

One of the main tasks is to investigate other fire types, but solely TF5. In this contribution, it was chosen as one of the simplest. However, especially in case of weak thermal drivers, like in case of smouldering, the dynamics will be more challenging to be captured and the gained spatial resolution will be of high importance for model validation.

To address the question of homogeneous layers, multiple LED strips and two (or more) cameras can be used. This will allow investigating the variations along the smoke layers. In combination with additional MIREX measurements at multiple heights, a wider understanding of the smoke spread, for example, light extinction coefficients, will be achieved. The precision of the measurements so far is limited by the production quality and potentially strong temperature dependence of the used commodity LEDs. Future experiments will be conducted with more stable devices accompanied with a study of the impact of temperature on luminosity and emission spectrum.

Further measurements of other quantities, like gas temperatures, will help to investigate other effects, like refraction. More information on the particles, using measurements of particle density and size distribution at few locations in the compartment during the fire, will allow to estimate the extinction cross-sections. In this way, different particle types, due to different combustion, pyrolysis or transport processes, will be distinguished for the various fire types. Thus, this information can be used to estimate the particle numbers, with the assumption of a known c_{ext}, as well as the difference of infrared and red light measurements. In addition, there exist already approaches to characterise the particle properties based on their interaction with light at three selected wavelengths.[18,19] Similar analysis will be conducted with the presented method.

Finally, numerical simulations with FDS will be carried out. The results of these simulations will be used to investigate the homogeneity assumptions in combination with a comparison the measured (LED and MIREX) extinction coefficients. In case of fire-type TF5, all relevant quantities, like the mass loss rate, have been captured. Thus, a design fire will be sufficient to represent the evaporation process.

ORCID

Lukas Arnold https://orcid.org/0000-0002-5939-8995
Alexander Belt https://orcid.org/0000-0002-6091-9321

REFERENCES

1. Erik Andresen. *Wayfinding and Perception Abilities for Pedestrian Simulations* (PhD thesis). Bergische Universität Wuppertal; 2018.
2. Leonard YC. A concept for estimating available safe egress time in fires. *Fire Safety J*. 1983;5(2):135-144.
3. Węgrzyński W, Vigne G. Experimental and numerical evaluation of the influence of the soot yield on the visibility in smoke in CFD analysis. *Fire Safety J*. 2017;91:389-398.
4. Benjamin Schröder. *Multivariate Methods for Life Safety Analysis in Case of Fire* (PhD thesis). Bergische Universität Wuppertal; 2016.
5. Benjamin Schröder, David Haensel, Mohcine Chraibi, Lukas Arnold, Armin Seyfried, and Erik Andresen. Knowledge- and perception-based route choice modelling in case of fire. Paper presented at: Proceedings of the 6th International Symposium on Human Behaviour in Fire; vol 2015, 2015.
6. Kevin McGrattan, Simo Hostikka, Randall McDermott, Jason Floyd, Craig Weinschenk, and Kristopher Overholt. Fire dynamics simulator user's guide, version 6; July 1, 2019.
7. Hamins A, Maranghides A, Johnsson R, et al. *Report of Experimental Results for the International Fire Model Benchmarking and Validation Exercise 3*. Vol 1013. Gaithersburg: NIST Special Publication; 2003.
8. Gottuk D, Mealy C, Floyd J. Smoke transport and FDS validation. *Int Assoc Fire Safety Sci*. 2008;9:129–140.
9. Jin T. Visibility through smoke. *J Fire Flammab*. 1978;9:135–155.
10. Bouguer P, Middleton WE. *Optical Treatise on the Graduation of Light: Translated, with Introduction and Notes by W. E. Knowles Middleton*. Toronto, Canada: University of Toronto Press; 1961.
11. Mulholland GW. Chapter smoke production and properties. *SFPE Handbook of Fire Protection Engineering*. 3rd ed. New York, NY: Springer; 2002.
12. Newman JS, Yee GG, Paul S. Chapter smoke characterization and damage potentials. *SFPE Handbook of Fire Protection Engineering*. 5th ed. New York, NY: Springer; 2016.
13. CERBERUS LTD. Extinction measuring equipment MIREX. Technical description; 1991.
14. George WM. How well are we measuring smoke? *Fire Mater*. 1982;6 (2):65-67.
15. Putorti AD. Design parameters for stack-mounted light extinction measurement devices (NISTIR 6215). Technical report; 1999.
16. Tuomo Rinne, Jukka Hietaniemi, and Simo Hostikka. Experimental validation of the FDS simulations of smoke and toxic gas concentrations. VTT Technical Research Centre of Finland Ltd, Working Papers, vol 66; 2007.
17. The European Committee for Standardization. EN 54— Fire detection and fire alarm systems, part 7: smoke detectors point detectors using scattered light, transmitted light or ionization; 2000.
18. Cashdollar K, Lee C, Singer J. Three-wavelength light transmission technique to measure smoke particle size and concentration. *Appl Opt*. 1979;18:1763-1769.
19. Flecknoe-Brown KW, Van Hees P. Obtaining additional smoke characteristics using multi-wavelength light transmission measurements. Paper presented at: proceeding of the Fire and Material Conference 2015; February 2–5, 2015; San Francisco. https://www.interscience comms.co.uk/html/conferences/fm/fm15/fm15.htm.

How to cite this article: Arnold L, Belt A, Schultze T, Sichma L. Spatiotemporal measurement of light extinction coefficients in compartment fires. *Fire and Materials*. 2021;45:1075–1084. https://doi.org/10.1002/fam.2841